Permeability evolution during progressive deformation of intact coal and implications for instability in underground coal seams

Shugang Wang [a,*], Derek Elsworth [a], Jishan Liu [b]

[a] Department of Energy and Mineral Engineering, G3 Center and Energy Institute, The Pennsylvania State University, University Park, PA 16802, USA
[b] School of Mechanical and Chemical Engineering, The University of Western Australia, 35 Stirling Highway, Crawley, WA 6009, Australia

ARTICLE INFO

ABSTRACT

We report measurements of deformation, strength and permeability evolution during triaxial compression of initially intact coals. Permeability is continuously measured by the constant pressure differential method, together with axial and volumetric strains for both water (H_2O) and strongly adsorbing carbon dioxide (CO_2) gas. Strength and Young's modulus increase with increasing confining stress and permeability is hysteretic in the initial reversible deformation regime. As deviatoric stress and strain increase, permeability first decreases as pre-existing cleats close, and then increases as new vertical dilatant microcracks are generated. Post-peak strength the permeability suddenly increases by 3–4 orders-of-magnitude. During loading, the inflection point where permeability begins to increase occurs earlier than the turning point of volumetric strain, which may be explained by the competing processes of axial crack opening and closure of oblique and transverse cracks. The generation of these vertical microcracks does not enhance gas migration in the horizontal direction but will accelerate the rate of gas desorption and weaken the coal.

Based on this mechanistic observation, we propose a process-based model for bursting in underground coal seams. Horizontal and vertical stresses redistribute ahead of the mining-face immediately after the excavation and influence pore pressure, permeability, and desorption rate. Due to this redistribution, the zone closest to the mining-face may experience tensile failure. Interior to this zone a region may develop with gas overpressures induced by desorption and this may contribute to the occurrence of coal and gas outbursts. Beyond this, an overstressed zone may initiate shear failure driven by gas pressures if the desorption rate outstrips the rate of drainage. We discuss the implications of this on the instability of coal seams to CO_2 injection and the potential for induced fault slip.

1. Introduction

Experimental constraints on the evolution of permeability of coal concurrent with deformation are fundamental in understanding fluid flow within underground coal seams. Fluid flow is important in influencing strength and stability of coal seams and in determining failure processes such as coal bumps and gas outbursts in underground coal mines [1] and possible fault reactivation induced by deep underground injection of CO_2 [2]. In the last 150 years, perhaps over 30,000 outbursts have occurred worldwide, resulting in significant damage and numerous and fatalities [1,3–5]. Despite extensive research into violent failures in coal mines, surprisingly little progress has been made in the past century in improving our understanding or towards prediction. Partial alleviation of outbursts by control measures

has been widely achieved. These include in-seam gas pre-drainage ahead of mine development [6], hydraulic fracturing [7] and high-pressure waterjet techniques [1,8,9]. However, no entirely satisfactory methods are known [10]. As mines progress into deeper and gassier coalbeds, the prediction and prevention of these low-probability/high-consequence events is of utmost importance for the coal mining industry worldwide.

The causes of instantaneous gas outbursts are complex and investigations have typically been limited to specific aspects—mainly as a result of significant constraints in acquiring reliable data. Various models and mechanisms have been proposed to explain the complex processes involved in bursts and bumps [1,3]. These include spatially-zoned and sequential failure models identifying response [5]. These models have a common feature in that a spatial variation of stresses, gas pressures, damage, permeability, and desorption rate exists ahead of the mining face in underground coal seams. This is due mainly to the sudden stress redistribution induced by mining [11]. Changes in one zone influence adjacent zones and are of great consequence in controlling the stability of coal seams. But also

* Corresponding author. Tel.: +1 281 795 9479.
E-mail addresses: shugangwang@gmail.com, szw138@psu.edu (S. Wang).

coupling of the effects of stress, permeability and desorption provide a potential positive feedback to the liberation of gas. Therefore an understanding of the evolution of sorptive capacity (generating gas as stress increases) and permeability (dissipating gas as stress increases) provides important control on this process. Experimental measurements of these effects are crucial in understanding the response where the coal seam ahead of the mining face is loaded by the approaching face.

Measurements on coal have investigated the evolution of strength and the stress–strain characteristics in triaxial compression [12–14], scale effects on strength [14–16], the evolution of elastic parameters [17], the influence of width/height ratio on post-failure behavior [18] and the dependence on loading rate [19]. Permeability of intact coal has been studied as a function of applied stress [20–26] and of pore pressure and of fluid composition [26–28]. Generally, permeabilities to water and gases decrease with increasing effective stress before new fractures are generated. Permeabilities to sorbing gases such as methane and carbon dioxide are controlled by both poromechanical and sorption-induced swelling effects [29,30]. The difference in permeabilities for intact coal samples and discretely fractured samples is sometimes larger than 3 orders-of-magnitude [26], suggesting a similar anticipated difference between permeabilities of coals pre- and post-failure. Although the failure characteristics and permeability evolution of coals are examined and reported frequently, these aspects are typically examined separately and in isolation. Experimental determination of permeability evolution of coals during progressive deformation has received remarkably little attention. The interactions of coal deformation, cleat closure, the creation of damage and of new fractures and the generation and dissipation of fluid (gas and liquid) pressures are inherently related to the coupled mechanical and transport properties of coal. Indeed, progressive loading influences the permeability of coal and that in turn affects the rate and pattern of deformation and failure. For instance, with the presence of sorbing gases, coal fracturing generates new fracture surfaces, accelerates the gas desorption, releases internal energy and may promote a feedback to runaway failure. This highlights the importance of understanding the relationship between progressive damage and permeability evolution.

Previous studies have identified the role geological structures such as deformed zones of strike-slip, thrust, reverse, and normal faults, rolls, and slips on the occurrence of outbursts [1,3–5,10,31–33]. These narrow deformed zones, whether at large or small scale, form the loci for stress and gas concentration, within which coal has been physically altered into cataclastic, granular, or mylonitic microstructures [33]. The presence of these faults is considered as one essential factor for the occurrence of outbursts. Therefore, outburst-prone zones may be screened by studying the spatial distribution of altered coal and geological structures and the related spatial evolution of permeability [5,31]. With the increasing interest in sequestrating CO_2 into deep underground coal seams, a lack of knowledge exists on how permeability changes temporally and spatially with injection-induced stress redistribution and how these changes affect the stability of coals. Fluid flow is controlled by both the bulk transport properties of the coal matrix as well as heterogeneities such as cleats at small scale and faults at large scale. The distribution of fractures on all scales affects the permeability and desorption response and is crucial in understanding the response to applied loading.

2. Experimental technique

The experimental apparatus used in these experiments is shown schematically in Fig. 1. A triaxial core holder is capable of accepting membrane-sheathed cylindrical samples (2.5 cm diameter and 10 cm long) and of applying independent loading in the axial and radial directions. Confining and axial stresses up to 35 MPa are applied by a dual cylinder syringe pumps with control resolved to ±1 kPa. Constant upstream pressure is applied by a third syringe pump with the downstream reservoir open to the atmosphere to measure both water and gas permeabilities down to 10^{-23} m². Temperature control jackets are used for the hydraulic pumps to maintain fluid temperature to within ±0.1 °C. Axial displacement is measured externally using a linear variable displacement transducer (LVDT) in contact with the moving piston to a resolution of ±1 µε. Radial displacement is
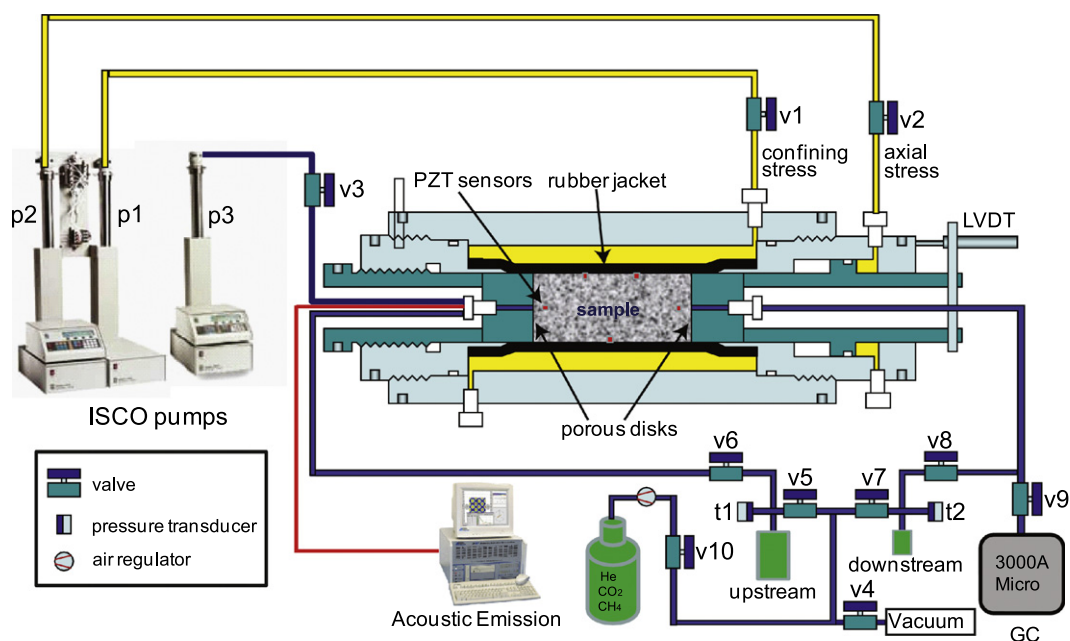

Fig. 1. Schematic diagram of the experimental apparatus. The constant pressure differential technique is used to measure permeability evolution during progressive axial deformation.

measured from volume change in the confining fluid also to $\pm 1\ \mu\varepsilon$. The stiffness of the loading system is 85 kN mm^{-1} (at zero confining stress) and the axial displacement of the sample is obtained by subtracting the displacement of the loading system from the apparent displacement measured by the LVDT. Axial strain is then calculated with reference to the initial length of the sample.

The cylindrical sample is sandwiched within the Temco core holder between two cylindrical stainless steel loading platens with through-going flow connections and flow distributors. The sample and axial platens are isolated from the confining fluid by a polyvinyl chloride (PVC) rubber jacket. Pressure, flow rate, and changes in fluid volume of the confining fluid are recovered from the ISCO pumps and recorded via (National Instruments) Labview. Output signal from a single LVDT is converted at 16-bit resolution using a 16-channel data acquisition system. All signals are logged digitally at a sampling rate from 1 Hz to 1 kHz.

We apply a constant 1 MPa upstream pore pressure and open the downstream effluent port to the atmosphere to maintain a constant pore pressure differential (1 MPa) between the two ends of the samples. The permeability k of the sample to water can be determined using Darcy's law as,

$$k = \frac{\mu L}{A} \frac{q}{\Delta P} \tag{1}$$

where ΔP is the pressure difference across the sample, L is the length of the sample, μ is viscosity of the fluid, q is the flow rate, and A is the cross sectional area of the sample.

For compressible gas, fluid expansion affects the permeability measurement. Assuming that gas permeation through the sample is an isothermal process, and that the ideal gas law applies, the gas permeability can be calculated from [25]

$$k = \frac{\mu L}{A} \frac{2P_0 q_0}{P_2^2 - P_1^2} \tag{2}$$

where subscripts 1 and 2 denote the downstream and upstream conditions, respectively.

Permeability measurements in tight rocks and coals can be influenced by gas slippage at the pore wall—the Klinkenberg effect [25,27,34,35]. When the mean free path of the gas molecules is of the same order as that of the flow path dimension, the gas molecules have appreciable interaction (i.e., collisions) with the flow path surfaces. The relation between measured permeability k_m in the case where slip occurs and the absolute permeability k is given as:

$$k_m = k\left(1 + \frac{b}{P}\right) \tag{3}$$

where k is the absolute gas permeability under very large gas pressure where the Klinkenberg effect is negligible (m^2) and b is the Klinkenberg coefficient (Pa) that depends upon the mean free path of the gas molecules. This in turn, depends on gas pressure, temperature, and molecular weight of the gas. In this study, the Klinkenberg effect is subtracted from all permeability data with $b = 0.76 \times 10^6$ Pa.

The experiments were performed on high volatile bituminous coal from the Gilson Seam (Book Cliffs, Utah) recovered as a large block from a depth of 548 m. The mean density of the coal under unconfined conditions was calculated from the mass and volume of the cylindrical cores. This procedure yielded an average matrix density of 1189.2 kg m^{-3}. Table 1 summarizes the proximate analysis and physical properties of the coal. The gas used in this study is CO_2 at a purity of 99.995%.

3. Results

3.1. Triaxial compression tests

The experimental details for all of the tests reported are summarized in Table 2. In this section, results are presented for permeability evolution during progressive deformation until ultimate failure of the coal samples at various effective pressures. To investigate permeability hysteresis with strain history, one sample was also subjected to monotonically increasing-amplitude cyclic loading (see Table 2). This consisted of 6 incremented then decremented stress steps with increasing axial stresses to 7 MPa, 12 MPa, 17 MPa, 22 MPa, 27 MPa, 34 MPa. All experiments ended in localized brittle failure of the sample in the form of a through-going shear fracture (Fig. 2).

Fig. 3 shows the change in both (a) deviatoric stress and (b) permeability versus axial strain for five tests completed at effective pressures of 0.75 MPa, 1.5(2) MPa, 2.25 MPa, and 3 MPa. The stress–strain curves show typical behavior for coal with strength increasing with increasing effective confining stress. For the first 5 MPa of loading the stress–strain response is first concave upward and then becomes linear-elastic up to the yield point. The yield point is taken at the departure from the linear segment where behavior is then concave downwards until the peak stress (for tests T3564, T3566, and T3567). For tests T3563 and T3568, a step increase in axial strain is apparent in the linear-elastic segment, beyond which the stress–strain relation is still

Table 1
Properties of the used Utah bituminous coal.

Proximate analysis		
Fixed carbon	Volatile matter	Ash
53.97%	37.02%	3.02%

Ultimate analysis				
Carbon	Hydrogen	Nitrogen	Sulfur	Oxygen
81.75%	3.77%	1.35%	0.50%	12.62%

Vitrinite reflectance
0.53

Table 2
Summary of the conditions and key results from the experiments.

Test No.	Length (cm)	Density (kg m^{-3})	P_c (MPa)	P_p (MPa)	P_{eff} (MPa)	Young's Modulus (GPa)	Peak Stress (MPa)	Axial Strain at failure	Initial permeability (m^2)	Final permeability (m^2)	Fluid type
T3566	5.00	1174.2	3.5	0.5	3	2.04	32.23	1.73%	8.81e−19	1.10e−14	CO_2
T3567	4.10	1198.6	2.75	0.5	2.25	1.54	26.9	2.06%	7.72e−19	8.03e−15	CO_2
T3563	5.08	1173	2	0.5	1.5	1.26	21.25	1.74%	1.53e−18	1.92e−14	H_2O
T3564	5.97	1182.1	2	0.5	1.5	1.77	21.47	1.39%	6.86e−19	5.10e−14	CO_2
T3568	3.96	1210.5	1.25	0.5	0.75	1.10	19.4	2.09%	6.00e−17	9.19e−15	CO_2
T3569[a]	4.39	1196.8	2	0.5	1.5	1.34[b]	33.75	1.73%	3.35e−18	2.41e−15	CO_2

[a] Test T3569 was cycled.
[b] Calculated from the first cycle.

Fig. 2. Photograph of a fractured sample with a through-going shear fracture representing the failure mode.
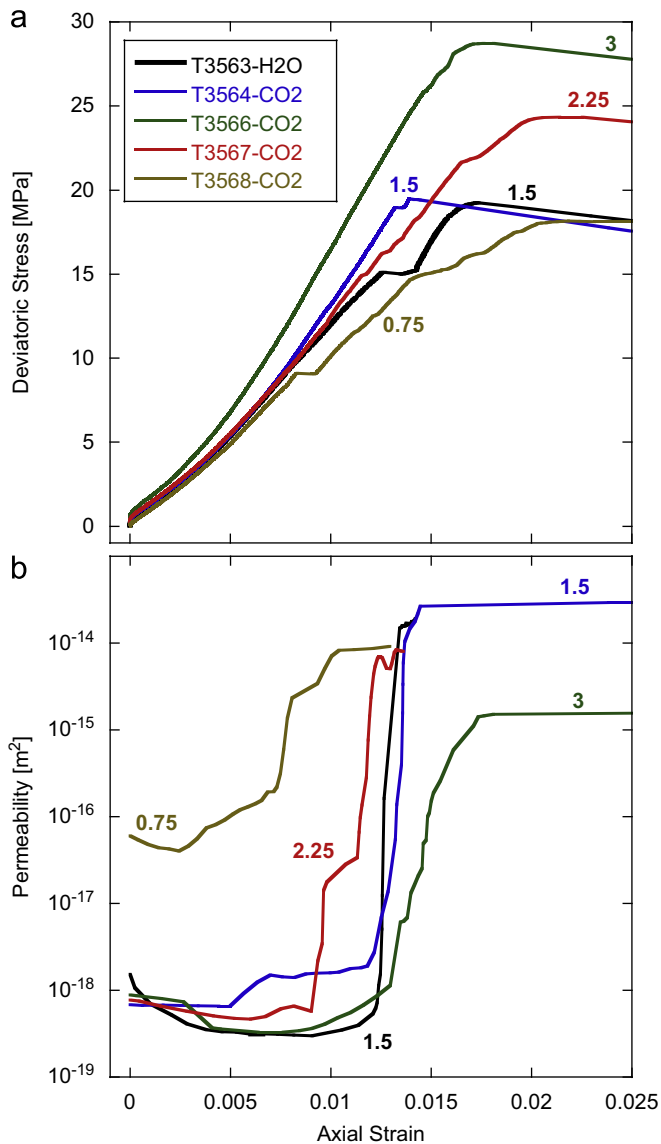

Fig. 3. (a) Deviatoric stress versus axial strain and (b) permeability versus axial strain. Effective confining stresses are indicated and pore fluid pressure (deionized water or CO_2) was maintained at 0.5 MPa. Test numbers refer to those used in Table 1.

linear. This feature indicates the generation of micro-crack(s) as a consequence of loading—an hypothesis that is confirmed by the permeability results. Peak stresses leading to failure are $\sim$19 MPa, 21 MPa, 27 MPa, and 32 MPa for effective stresses of 0.75 MPa, 1.5 MPa, 2.25 MPa, and 3 MPa, respectively. For all experiments, axial strain at failure ranges from $\sim$1.4% to $\sim$2.1%. Sample failure occurs rapidly after the peak stress is reached with a significant increase in strain. As shown in Fig. 3(a) and in Table 2, under the same confining stress of 1.5 MPa, the specimen infiltrated by H_2O (T3563) has a lower Young's modulus and a slightly lower strength than the one infiltrated by CO_2 (T3564), which may infer that water has a larger weakening effect based on these two tests.

Except for sample T3568 that has a visible fracture sub-parallel to the loading direction (flow direction), initial permeabilities for all other samples (hydrostatic loading only) are bounded to within one order of magnitude (from 6.86×10^{-19} m² to 3.35×10^{-18} m²). As strain increases, permeability initially decreases for all effective pressures up to a strain ranging from 0.0024 (T3568) to 0.0072 (T3566) for tests with CO_2 as the permeant, and 0.0091 (T3563) for water. This trend is consistent with the concave upward section of the stress–strain curve. After this initial decrease, permeability gradually increases up to at a strain of $\sim$1% where either microcracks are generated or existing natural fractures are dilated in shear. In this condition permeability increases by less than one order of magnitude (from 6.54×10^{-19} m² to 2.74×10^{-18} m² for T3564). Ultimately, permeability increases sharply by two to three orders of magnitude when a large axial fracture is induced prior to macroscopic failure (from 2.74×10^{-18} m² to 5.10×10^{-16} m² for T3564).

Fig. 4a shows the evolution of volumetric strain and Fig. 4b shows the evolution of permeability with deviatoric stress. The axial and radial strains include the effects from the change in crack volume, elastic strain of the solid grains, and sorption-induced swelling or desorption-induced shrinkage. Strains are positive in compaction. As expected, the stress–permeability behavior is similar to that for strain–permeability (Fig. 2). For all tests, the sample volume initially decreases to a maximum compactive strain and then begins to dilate at an accelerating rate. One key observation is that the inflection point of the volumetric strain–stress curves, i.e., where the samples stop compacting and start dilating, does not coincide with the inflection point of the permeability–stress plot. Permeability begins to rapidly increase at an appreciably lower strain—and this is slightly before the change from net compaction to dilation. Dashed lines and stars are added on the data of test T3568 to illustrate this observation. It is clearly seen that the inflection point of the permeability is ahead of that of volumetric strain. It is worth noting that coal is such a material that each specimen has a unique cleat system. Therefore heterogeneity will influence any mechanical or transport behavior. This turning point increases with an increase in effective confining stress. The peak volumetric strain, i.e., the maximum decrease in sample volume, also seems to vary as a function of effective pressure, with the largest volumetric strain of around 0.0036 recorded for an effective confining stress of 0.75 MPa.

Fig. 5 shows the evolution of deviatoric stress and permeability with time for tests with CO_2 as the permeant. The solid lines represent deviatoric stress versus time and the dotted lines represent permeability versus time. The interpretation of the postfailure permeability data is not straightforward as the specimens will have developed different strains and failure plane structures during the deformation and failure processes. The postfailure permeability is primarily controlled by the characteristics of the failure plane. Thus the variation in postfailure permeability is largely dependent on the width and shape of the through-going fracture. However, it can be
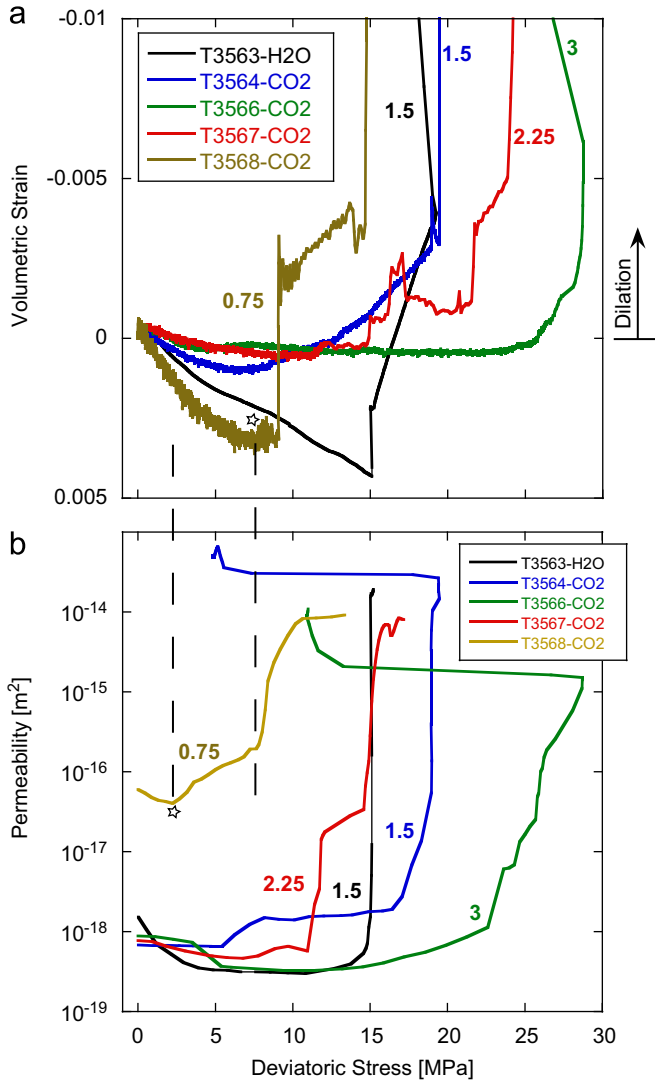
Fig. 4. Evolution of (a) volumetric strain and (b) permeability with deviatoric stress. Effective confining stresses are indicated and pore pressure was maintained at 0.5 MPa.

seen that postfailure permeability is much higher than the initial permeability. For an effective pressure of 1.5 MPa, permeability reaches 1.1×10^{-14} m^2 which is 4 orders of magnitude greater than the initial preloading permeability. The test with the lower effective stress has a larger change in permeability between post- and pre-failure states.

3.2. Increasing deviatoric stress amplitude cyclic loading test

In order to examine the effects of permeability hysteresis due to loading and unloading by deviatoric stress we conducted one cyclic loading test. The deviatoric stress was incremented then decremented over six cycles. Observations from the cyclic loading may have implications on what effect such loading and unloading histories may have on in situ coal seams that undergo loading cycles due to mining-induced stressing.

Fig. 6a shows the applied cyclically increasing deviatoric stress and resulting axial strain versus time. The sample was cyclically-loaded to five peak axial stresses (7 MPa, 12 MPa, 17 MPa, 22 MPa, 27 MPa), unloaded to 3 MPa and failed on the final cycle. Fig. 6b shows the evolution of permeability concurrent with volume strain—each shown versus time. For the first four cycles an increasing residual strain (compaction) accumulates after each
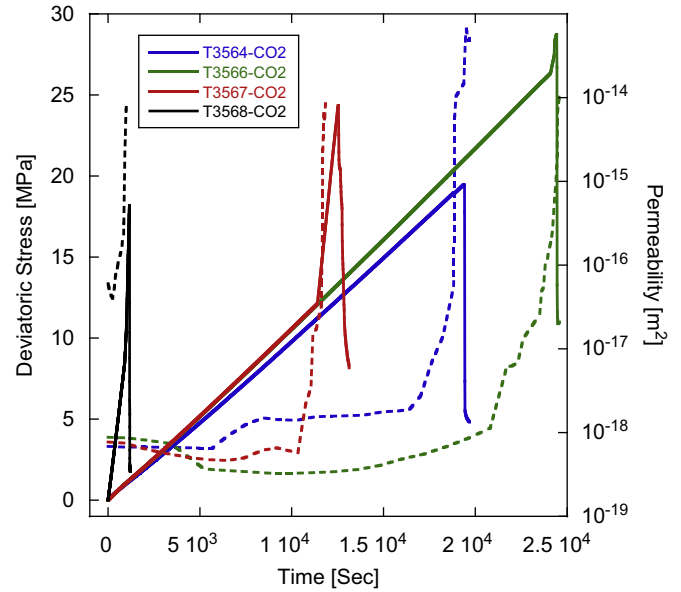

Fig. 5. Experimental data for tests with CO_2 as the permeant. The deviatoric stress and permeability are plotted versus time. Pore fluid pressure was maintained at 0.5 MPa.

unloading (Fig. 6b). Similarly, for the first three loading cycles the minimum permeability at peak stress and recovered permeability each decrease monotonically with the number or cycles (Fig. 6b). This suggests that the deviatoric stress is insufficient to promote the development of fresh microcracks—rather, damage accumulates across cleats. Permeability at the end of the fourth loading cycle begins to increase, suggesting dilation of preexisting cleats or the generation of new microfractures either parallel or sub-parallel to the axial stress direction. During the fifth and sixth cycles, permeability begins to increase during loading, indicating the generation of new fractures—this is congruent with the change from compaction to dilation within the mechanical response. The sampled fails on the sixth cycle with the final post failure permeability three orders of magnitude higher than the initial permeability (2.41×10^{-15} m^2).

Fig. 7 shows the evolution of prescribed deviatoric stress and permeability with axial strain for the cyclically loaded sample. The solid lines represent deviatoric stress versus axial strain and the dashed lines represent permeability versus axial strain. Three characteristic features are apparent in the permeability–stress response. These are: (1) non-linearity at low stress; (2) a range of elastic linearity of stress with strain; and (3) irrecoverable axial strain upon unloading. At low stresses (< 5 MPa deviatoric stress), the stress–strain curve is strongly nonlinear and Young's modulus increases as stress is increased. Eventually a stress is reached beyond which the stress–strain curve becomes approximately linear. In addition to nonlinear elastic behavior, an elastic hysteresis is observed. On unloading, a finite stress change is needed before the direction of slip at the crack interface is reversed and therefore the unloading modulus is initially greater than the loading modulus as shown by the difference in slopes of loading and unloading curves. The nonlinear elastic behavior of coals under triaxial compression can be attributed to the presence of preexisting cleats. At low stresses the cleats are initially open and close as the stress is increased, resulting in the stiffening of the fracture–matrix composite. Once the cleats are fully closed, the stiffness of the material remains constant.

The elastic hysteresis can also be explained by the presence of cleats and the effect of friction between cleat surfaces. The Young's modulus of the elastic portion of each cycle grows for
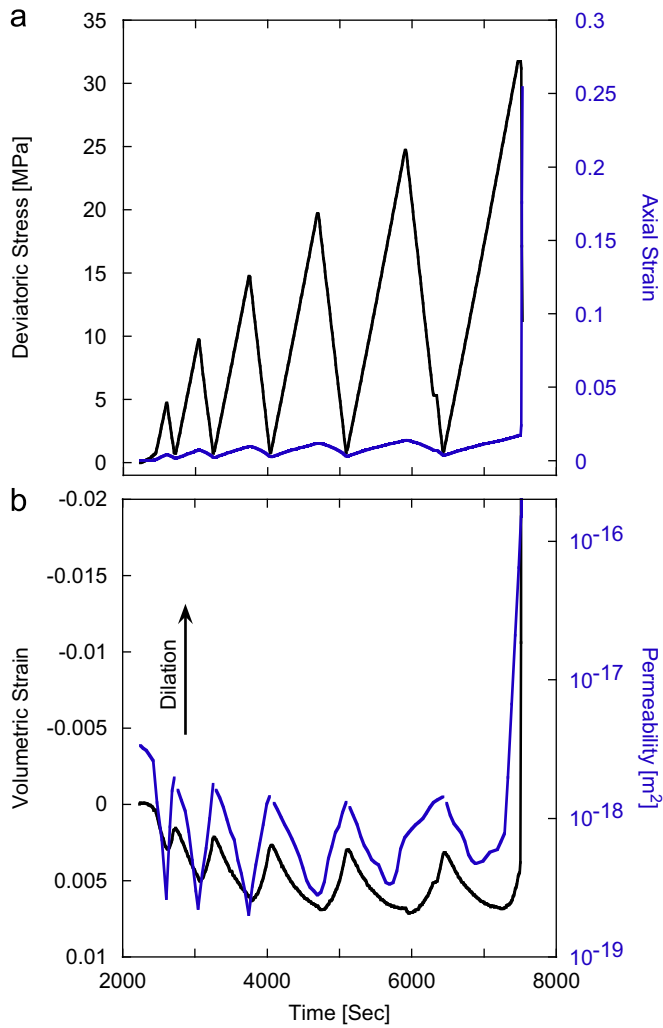
Fig. 6. Experimental data for cycled deviatoric stresses. Pore fluid pressure (CO_2) was maintained at 0.5 MPa with a confining pressure of 2 MPa. (a) Deviatoric stress and axial strain versus time. (b) Volumetric strain and permeability versus time.
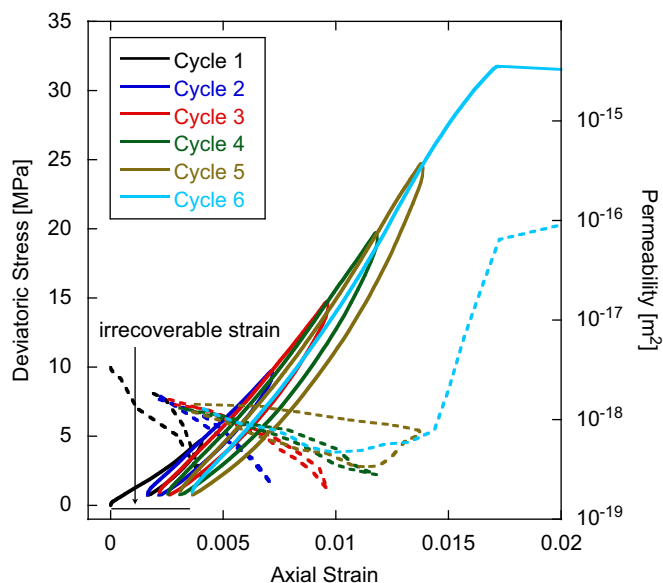

Fig. 7. Deviatoric stress (solid) and permeability (dotted) versus axial strain for cycled loading. Pore fluid pressure (CO_2) was maintained at 0.5 MPa with a confining stress of 2 MPa.
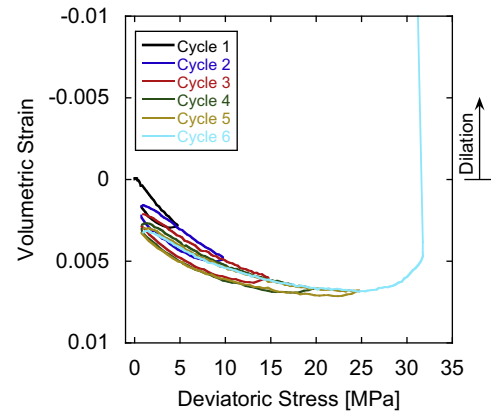

Fig. 8. Volumetric strain versus deviatoric stress for cyclic-loading. Pore fluid pressure (CO_2) was maintained at 0.5 MPa with a confining stress of 2 MPa.

each of the first three cycles then remains nearly constant on subsequent cycles. Each cycle has an irrecoverable axial strain after unloading that may be due to the closure of existing cracks in the previous cycle. For the first four cycles, permeability decreases with increasing strain (loading) and recovers with decreasing strain (unloading). Permeability values for all other cycles are nearly equal after the unloading, which are lower than the initial preloading permeability magnitude. Permeability evolution during loading–unloading–reloading cycles follows different paths indicating a hysteretic phase. This may be attributed to the same rationale as for elastic hysteresis. In the fifth cycle, permeability begins to increase with increasing axial strain. This may be an indication of the generation of new cracks or the dilation of preexisting cleats. In the final cycle, permeability gradually increases with strain until the sample fails and permeability is augmented by more than three orders of magnitude.

Fig. 8 shows the evolution of volumetric strain as a function of deviatoric stress for cyclic loading. As stress is raised in each of the first five cycles, the sample continues to compact but at a decreasing rate. Volumetric strain also shows a hysteresis with irrecoverable strain remaining upon unloading for each cycle. At high deviatoric stress, the sample starts to dilate gradually (at 25 MPa) prior to sudden macroscopic failure (at 32 MPa) with related instantaneous dilation.

4. Analysis for coal seams

In this section we relate our experimental data to underground coal seams subjected to mining-induced stresses. Permeability evolution during static and cyclic deviatoric loading is discussed and the feedbacks of these changes on deformation and failure are explored. We present an ensemble model for strength and permeability evolution and discuss its implication on fluid flow and rupture in coal seams and in particular with reference to instantaneous gas outbursts and CO_2 sequestration.

4.1. Failure characteristics

In this work we define the yield stress as the stress at the limit of proportionality of the deviatoric stress–axial strain curve (the nonlinear inflection). Both the fracture stress and the yield stress were observed to increase with an increase in confining stress from 0.75 MPa to 3.5 MPa. This is consistent with earlier studies [12–14]. The fracture stress increases in a roughly linear manner, as shown in Fig. 9. Tests under the confining stress conditions of this study have shown that the coal is an elastic, brittle-plastic
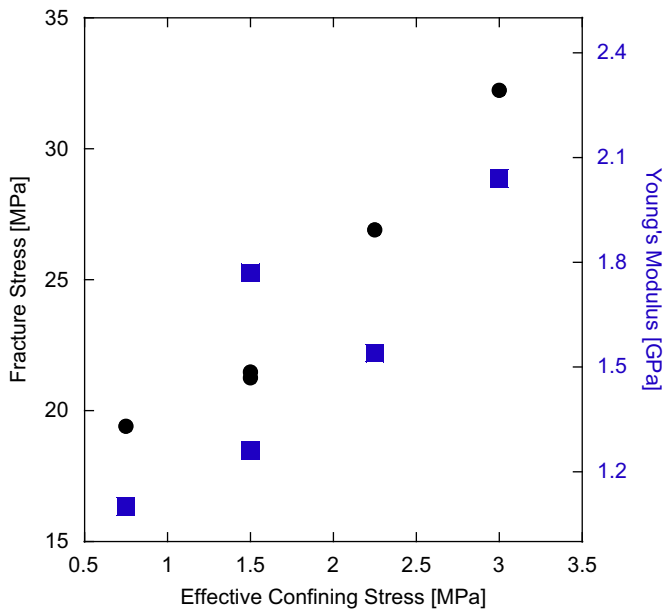
Fig. 9. Fracture stress and Young's modulus as functions of effective confining stress.

material with strain-weakening. Aside from some non-linearity associated with crack closure at lower stresses, non-linearity is only observed at stresses in excess of about 85% of the peak strength of the coal—similar with other observations [17].

In general three features are evident on the stress–strain curve [13,14,36]. These are: (1) an initial non-linear portion of the stress–strain curve caused by the closing of the preexisting cleats in the coal; (2) a range of elastic linearity of stress with strain from which the Young's modulus in compression can be determined; (3) A final non-linear portion of the stress–strain curve due to pre-rupture cracking. The values of the Young's modulus of the coals tested are given in Table 1. The Young's modulus increases with increasing confining pressure as shown in Fig. 9. The change in the observed Young's modulus with confining stress is probably due to compaction of the coal matrix, the increasing stiffness of the cleats with stress and the difference in sorption capacities with stress.

Acoustic emission (AE) techniques have been used in the laboratory to image how coal and rocks fail with time [37–39]. Generally, at low stress, AE events are broadly distributed throughout the sample, indicating that the deformation is quasi-homogeneously distributed within the sample. With increasing deviatoric stress and the generation of new axial cracks, AE counts and energy gradually increases prior to the failure of the sample when event rates increase drastically. In situ compression tests in coal mines also show that the failure is associated with gradual opening of vertical cleats and spalling from one or more faces, usually near a corner of the specimen [15].

Although the coal specimens used in this study of the same size, scale effects exist in coals. Generally, the strength and stiffness of coal decrease with increasing size [14–16]. Strength and post-failure stiffness both decrease with a decrease in the width/height ratio of the pillar [18]. Strength is relatively insensitive to loading rate with other factors creating greater scatter in the strength data [19].

4.2. Permeability evolution from triaxial compression tests

Gas flow in coal seams is commonly represented as a dual porosity system accommodating two serial transport mechanisms: diffusion through the coal matrix then laminar flow through the cleat system [26,30,40,41]. The permeability is primarily determined by the cleat aperture [26,30]. The change in cleat aperture is a function of effective stress and is largely reversible at low stresses where no damage occurs [26,30,42] and irreversible at higher stresses [43]. Simultaneously, coal swells when a sorbing gas (such as methane or CO_2) flows into and is adsorbed by the coal matrix and coal shrinks when a sorbing gas flows out and is desorbed. This swelling and shrinkage can change the cleat aperture and thus coal permeability [26,30,42]. Moreover, coal damage and fracture induced by progressive loading can alter the rate of gas adsorption/desorption and coal swelling/shrinkage. Thus, the net change in coal permeability is a function of the poroelastic response, swelling or shrinkage of the matrix and the damage or fracture induced by the applied stress.

All experiments in this study show that permeability decreases initially with increasing deviatoric stress and axial strain as observed previously [20,25,26]. This decline is attributed to the nonlinear increasing stiffness in the early stress–strain curve (low stresses). This most likely results from the closure of cleats oriented transverse to the axial stress direction. Cleat closure causes a decrease in porosity and related decrease in permeability. The confining stress plays a role in how these shear cracks will close and hence influences the evolution of permeability under deviatoric stress. These triaxial compression tests are conducted after 24 h of gas flow—thus the sorption process is believed to be nearly complete prior to the initiation of deviatoric loading. After the gas adsorption is completed, swelling or shrinkage will not occur again until the internal structure of the coal is changed (e.g., creating new fractures or closing existing fractures).Thus, swelling is not an influencing factor at this stage. The relative rates of pressure build-up due to the loading rate and pressure decline due to drainage is important for undrained tests and for in situ coal seams because this relationship controls the net change in pore pressure within the sample. If the rate of pressure-build up outstrips the rate of pressure decline, the net increase in pore pressure will reduce effective confining stress which can promote instability to the sample. Thus for the tests performed in this study the poroelastic influence on permeability is the primary mechanism for the low stress stage.

With increasing deviatoric stress, new fractures, favorably oriented along the direction of the maximum principal stress will be created. These will balance the decline in permeability driven by confinement and eventually change the net permeability from decline to increase [20,25]. It is worth emphasizing that the inflection point of the volumetric strain-time curves, where the sample stops compacting and begins to dilate, occurs later in time than the inflection point of the permeability-time plot. This suggests that permeability increases noticeably at an appreciably lower strain. This key phenomenon, as expected for naturally fractured coal with cleats [44] and also observed in crystalline rocks [45], implies that changes in permeability and porosity may not track in the same sense at the same time due to anisotropy of the material. Similarly, compaction and dilatancy are not mutually exclusive processes [45]. Cleats in orientations perpendicular to the axial stress continue to close while new dilatant cracks grow parallel to the axial stress. The new dilatant cracks contribute more to axial permeability than the compacting radial cracks. Hence, the permeability net increases while the sample is still compacting. An increment of permeability added in the direction of the maximum principal stress (vertical stress) will likely not aid drainage as much as the same increment applied in the horizontal direction. But the generation of axial cracks weakens the mechanical properties of coal and accelerates the desorption rate. This point has important implications for instability in underground coal seams. There is no clear trend on how effective confining stress influences the magnitude of

permeability prior to sample failure and the permeability–strain relation, again possibly due to the anisotropic characteristics of coal.

The post failure permeabilities of most of the samples (other than T3568) show an increase in permeability of approximately 4 orders of magnitude—this is caused by the generation of a through-going fracture (Fig. 2). This fracture acts as a conduit for fluid flow and will further open due to the rapid shear displacement after failure [46,47].

4.3. Permeability evolution from induced cyclic stressing

The coal tested in this study exhibits strain and permeability hysteresis when subjected to cyclic loading (Fig. 6) [e.g., 20]. The energy stored during loading is dissipated upon unloading through the opening of existing fractures or the creation of new cracks. Depending on stress level this may influence the evolution of porosity and permeability. The similarity in the size of the change in permeability for both stress-cycled and non-cycled samples implies that permeability is primarily controlled by the maximum stress that the sample has undergone. Thus, permeability evolution under loading may be estimated if the stress condition is known. As noted in this study, permeabilities at the end of the first three unloading cycles are very close, suggesting that cyclic loading does not create cleat damage at low stresses. At higher stress levels, damage is inferred to result due to the larger increase in permeability and that the change is irreversible. It is worth noting that, during the fifth loading cycle, only after the deviatoric stress exceeded the maximum stress of the fourth cycle (22 MPa), were microcracks generated and hence permeability increased. This behavior is analogous to the "Kaiser effect" and has been observed elsewhere [e.g., 48].

Before microcracks begin to be generated, the permeability–strain curves during loading and unloading generally exhibit a concave-down form (Fig. 7). At the same deviatoric stress, a slight increase in permeability is observed during the unloading process. This discrepancy may be due to the temporary dominance of the nonaxial cracks on the permeability [49]. The significant change in permeabilities of intact coal and fractured coal describes again the important role of fracture geometry in determining the bulk permeability of coal [26]. This role is of importance for flow in underground coal seams as the in situ cleat/fracture network is complicated [1,3].

4.4. The roles of CO_2 adsorption and coal swelling

CO_2 adsorption by coal is a complex physicochemical process. Coals are capable of adsorption, followed by absorption, and then structural rearrangement (relaxation of the macromolecular network) that affects both adsorption and absorption [50]. The sorption mechanism for CO_2 is believed to include both chemical adsorption, in which the adsorbate is bound to the solid surface by a direct chemical bond; and physical adsorption, in which adsorption occurs mainly due to van der Waals and electrostatic forces between the adsorbate molecules and the atoms composing the adsorbent surface [50]. Carbon dioxide is predominantly stored in a molecular adsorbed phase within micropores of the coal in the matrix [51,52], and the remaining as a free phase in the macropores, cleats and cracks [52]. It is also well known that coal swells when exposed to CO_2, possibly due to chemical, elastic, and adsorption thermodynamic effects [53–55]. The amount of swelling depends on a variety of parameters, including the structure and properties of coal, gas composition, confining stress, pore pressure, temperature, fracture geometry, and moisture content [26]. Weakening effects of gas sorption on the strength of coal samples is found in triaxial compression tests [26]. Wang et al.

[26] show that coal samples under extended exposure to CO_2 have a lower compressive strength when compared to coal samples under short duration of sorption. Hol et al. [56] observe microfracturing of coal due to interaction with CO_2 under unconfined conditions.

For the triaxial compression tests conducted in this study samples are saturated for 24 h prior to applying the deviatoric load. Thus we assume that adsorption and swelling are largely complete. Fig. 4a shows that a consistent decrease in the maximum sample compaction with increasing confining pressure can be observed. We note here that the measured volumetric compaction is the sum of the elastic compaction and desorption induced compaction. Therefore this trend is explained by noting that for the samples under lower confining stress, more CO_2 is adsorbed during the 24 h saturation [26,53] so that with the application of deviatoric loading a larger amount of the adsorbed CO_2 will be desorbed [53]. This effect in turn increases the resulting compaction. The larger sorption capacity at lower confining stress may also make a contribution to the reduction in modulus and strength of coal and thus influence the stability of coal seams.

5. Instability in coal seams

We consider the stress changes that may develop around an advancing mine face and the influence these may exert on the evolution of effective stress state driven by desorption and inhibited drainage. We develop a process-based model and apply scaling to quantify these potential effects.

5.1. Process-based model

A schematic of this geometry (Fig. 10a) represents the principal features of anticipated mining-induced changes in vertical stress, horizontal stress, pore pressure, bulk permeability and desorption rate. We use this to understand how these stress conditions and transport characteristics change with distance from the mining face and how these changes might contribute to failure. Immediately following excavation (at location a) the mining face is totally unconfined, so the horizontal stress and pore pressure in fractures on the face drop to near zero. With increasing distance from the face, horizontal stress gradually increases towards the initial in situ stress at location e and compacts the vertical cleats. The vertical stress at the mining face immediately after excavation may be assumed to be close to the original in situ stress, but increases rapidly with distance from the face due to the mining-induced stress abutment. This surcharge closes the horizontal cleats and approaches a peak stress at location c. The stress concentration factor at location c, defined as the ratio between the mining-induced stress and the pre-mining in situ stress, ranges from 1.5 to 6 [57–59]. The distance from the mining face to location c is strongly dependent on coal seam properties and geometry and can be from meters to tens of meters [11,59,60]. Beyond location c, the vertical stress gradually resets to the in situ stress. Permeability is largest at the mining face since the coal is unconfined and permeability is confining stress dependent [26]. With increasing distance into the face the increasing stresses compact the preexisting cleats and thus permeability decreases until location b is reached—and here micro-fractures are generated. In the zone between locations a and b, pore pressure in the fractures increases due to the drop in permeability and the original pre-mining gas pressure may be reset at location b. This increase in pore pressure decreases effective confining stress and hence has the potential to trigger
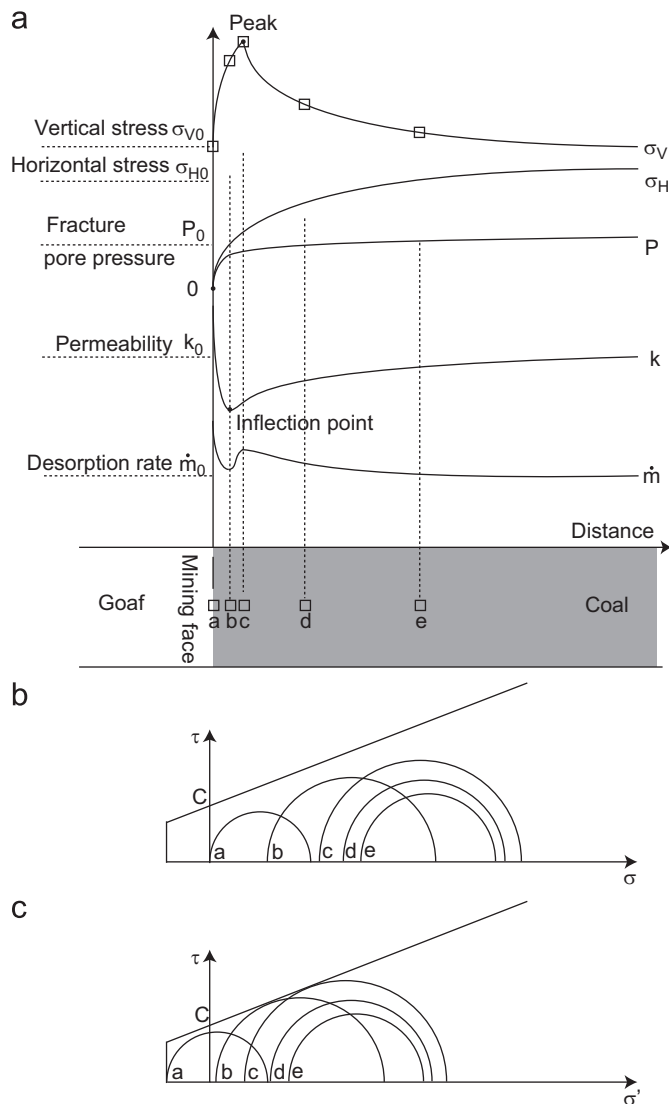
Fig. 10. Schematic diagram illustrating mining-induced stresses, pore pressure, permeability, and desorption rate ahead of the mining face. These conditions and properties are plotted as a function of distance from the mining face.

failure in the coal. Beyond location b, even though new microcracks are generated by the deviatoric load, these microcracks are parallel or subparallel to the vertical stress, as found in this experimental study. Thus the permeability is increased primarily in the vertical direction rather in the horizontal direction. The contribution to gas migration from these new cracks in the coal seam to the opening within the gob is insignificant. Beyond location c, permeability declines again with decreasing stresses to its original value. The rate of desorption depends on the local pressure difference between the matrix and the fracture [1,5]. On the mining face, since the matrix has a 3–4 order of magnitude lower permeability than the fracture, the pore pressure in the matrix remains almost the same while the pore pressure in the fracture rapidly drops to zero. Thus the maximum desorption rate occurs on the mining face where the largest pressure differential exists. With increasing distance from the face, this desorption rate decreases up to location b where new fractures are generated. These new fractures increase the volume of the fracture system and thus reduces the pore pressure in the fracture and then creates a local pressure differential between the matrix and the fractures hence promoting desorption. This is why the desorption rate increases at location b. The energy generated from gas

expansion due to the rapid desorption, together with the low horizontal permeability, microfracturing, and the fact that the coal is still under load, at location b, have potentially significant weakening effects on the coal. Rapid, energetic failure may result at this location.

Fig. 10b shows the progress towards failure for coal at these five locations without considering pore pressures. The positions of these Mohr circles show the relationship between deviatoric and confining stresses of the coal at these five locations. The coal at location a has zero confining stress and that at location e has the largest confining stress. The diameters of the Mohr circles illustrate the relative magnitude of deviatoric stress (the difference between vertical and horizontal stress) at these five locations. The coal at locations a and e support roughly the same vertical stress and point c is subject to the greatest vertical stress. We emphasize that these magnitudes are not absolute but are ranked in order of their relative magnitudes. We assume that without considering pore pressures within the fractures the coal at these five locations will not fail. Now we introduce anticipated pore pressures at these locations and investigate which regions will fail and how they will fail, as shown in Fig. 10c. At location a, we have assumed that the pore pressure decreases to zero immediately following excavation. However, if the permeability in this coal block is sufficiently low (of the order of 10^{-18} m²) [3] then the pore pressure may not drop to zero instantaneously (or may retain a strong gradient at the face) as the gas needs finite time to migrate out of the fractures. If pore pressures remain, this will cause a negative effective stress at location a with the Mohr circle translating across the zero normal stress axis, accordingly. Hence, coal at location a may experience a tensile stress as shown in Fig. 10c. Since the tensile strength of coal can be as low as 1 MPa [61], the coal at location a may undergo tensile failure. This failure may be categorized as tensile failure under rapid unloading. This unloading at a will increase the deviatoric stress at b, causing a decrease in permeability and a build-up in pore pressure due to inhibited gas migration. This increment in pore pressure reduces effective stress and thus shifts the Mohr circle to the left with the possibility of contacting the linear Mohr failure envelope. At location b, new microcracks will be created with these cracks either parallel or subparallel to the mining face (vertical stress direction)—they will not influence the horizontal permeability significantly. However, not only can these newly generated microcracks degrade the mechanical properties of the coal seams, they can also lead to rapid desorption of gas from the matrix which further accelerates failure. The loss of strength at this point can be both rapid and significant due to the high gas pressure that results from the rapid desorption of gas following coal failure. This failure may be categorized as gas overpressure in fractures and rapid desorption induced energetic failure [43]. The coal at location c is subject to the largest confining stress and vertical stress, and it has a slightly larger bulk permeability compared with coal at b. This is because both more new microfractures are generated and also a larger desorption rate results from the surface area generated by microcracking. With the increased vertical load, if the rate of desorption is less than the rate of gas migration, the coal will likely fail in shear without significant gas outbursts—this would be analogous to a bump resulting mainly due to the mining-induced vertical stress. If the desorption rate exceeds the rate of gas flow, however, the coal has the potential to fail energetically and catastrophically as an instantaneous coal and gas outburst.

This schematic model can be applied to coal seams under repeated mining-induced stress and with the presence of carbon dioxide and/or methane gases. With this model, we may understand why techniques such as in-seam gas pre-drainage ahead of mine development [6], hydraulic fracturing [7], and high pressure

waterjet techniques may suppress gas outbursts [1,8,9]. The pre-drainage of gas reduces the pore pressure within coal seams, increases the effective confining stress, and hence tends to stabilize the coal seams. Hydraulic fracturing can enhance the permeability of coal seams, especially in the horizontal direction, so that gas can migrate rapidly and increases the effective stress accordingly. However, this technique has a limitation in that fracturing can also weaken the properties of coal seams so it should be applied with caution. Beamish and Crosdale [1] report that as water content increases, the capability of the coal to accumulate elastic strain energy decreases and the permanent non-recoverable strain energy increases, and thus the energy index of liability to outburst decreases. The influence of water infusion could equally be explained using sorption isotherm results. With an increase in the coal moisture content at high pressure, the water molecules compete with those of methane for sorption sites and subsequently displace them, hence lowering the gas content of the coal. Aguado and Nicieza [8] suggest that the main purposes of water injection are to saturate the cleats and fractures so that methane emission can be hindered in the infused area, to divert the gas away from the face and to fracture the coal and partially relax the stresses that the coalbed is subjected to. Lu et al. [9] find that the waterjet technique is able to increase fractures, to reduce the internal stress, and to release the strain energy within the coal seam. Overall, the waterjet technique can increase fracture connectivity and permeability, and thus release internal energy and stored gas in fractures. The water molecules also compete with the CO_2 for sorption sites and subsequently displace them, hence reducing the adsorbed gas content in the coal matrix. When the coal seam undergoes mining-induced stress, the amount of gas that can be desorbed is reduced. So the magnitude of reduction in effective stress due to desorption will be decreased and this in turn helps stabilize the coal seam.

5.2. Scaling from the laboratory data to the field

The strength of coal is known to decrease with increasing specimen size [14–16] due to the presence of various discontinuities present within coal such as cracks, cleat and bedding planes. Based on the results of underground uniaxial tests on cubical coal specimens, a ratio of 7.6 was found between the strengths of 2 in and 60 in cubic specimens (edge dimension) (see Table 1 in [15]). In this study, we assume a ratio of 2 between the strengths of our laboratory specimen data and coal seams at depths corresponding to the confining stresses used in the experiments. This yields the Mohr circles and failure envelop shown in Fig. 11a. The Mohr failure criterion takes the form,

$$\tau = 2 + \tan 30^\circ \sigma' \tag{4}$$

where τ is the shear stress and σ' is the effective normal stress. The cohesion is 2 MPa and the internal friction angle is 30°.

We then construct Mohr circles based on the in situ stresses at a depth of 548 m, assuming an average density of 2500 kg m^{-3} for the overburden and a ratio of 0.7 between horizontal and vertical stresses. Then the in situ horizontal and vertical stresses are estimated at 9.6 MPa and 13.7 MPa, respectively, as shown by the smallest circle in Fig. 11b. With the mining-induced stress, the vertical stress reaches to 27.4 MPa, 34.25 MPa and 41.1 MPa for stress concentration factors of 2, 2.5 and 3, respectively. Based on the failure criterion derived above, we find that coal fails without the induction of pore pressure given a concentration factor of 3. For concentration factors of 2.5 and 2, pore pressures of 0.8 MPa and 3.9 MPa are needed to trigger the failure. Since gas pressure in the coal matrix is found to be as high as 6 MPa in underground coal mines [62,63] coal failure can occur for both cases. If the ratio between the strengths of laboratory data and coal seams is much
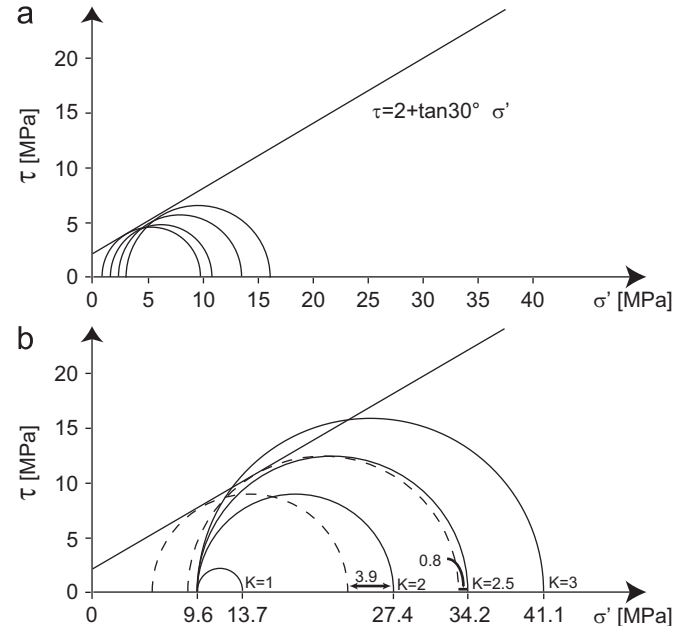

Fig. 11. (a) Mohr circles and failure envelop are constructed from the laboratory data for the underground coal seams under the same confining stress used in this laboratory study after considering the scale effect, (b) Mohr circles are plotted for the coal seams where coal samples were originally located. The confining stress is assumed constant at 9.6 MPa for all solid Mohr circles. From the left to the right, these represent in situ stresses, mining-induced stress with a stress concentration factor of 2, 2.5 and 3, respectively. The left and right dashed Mohr circle represent mining-induced stress with stress concentration factors of 2 and 2.5 after considering pore pressure effects, respectively.

larger than 2, which is likely to be the case (7.6 in [15]) then the seam may fail more readily under the same stress scenarios discussed above and significantly lower pore pressures are needed to prompt this failure.

We define the time interval between the point where new microcracks begin to be generated and the point where the final macroscopic failure occurs as the precursory time. As shown in Fig. 5, during each test, we measure and record permeability together with deviatoric stress and time simultaneously. The time when permeability starts to increase from decreasing is considered as the time when new microcracks begin to be created. Since we record the time when the specimen macroscopically breaks, we can calculate the time internal between these two events. The precursory time ranges from minutes to hours based on our experimental data, as shown in Fig. 12. The precursory time can be described as an inverse log function of the loading rate. This range of time intervals corresponds to the field observations such as in the Star mine, Idaho [64], in the Moonee Colliery, Australia [65] and mines in China [66]. We speculate that mining-induced stressing rate is site dependent and varies with overburden and coal seam properties. With practical experience in a particular mine, catastrophic failures can be possibly predicted minutes or hours earlier by using microseismic techniques that have been widely used for predicting roof failures, rockbursts, coal bumps and gas outbursts [6,10,39,64,67].

5.3. Implications for underground CO_2 sequestration

Long-term geologic sequestration of CO_2 in unmineable coal seams is one option to reduce CO_2 concentrations in the atmosphere [50]. Among the CO_2 sequestration or CO_2-ECBM pilot projects worldwide, the depths of these coal seams are usually ~1000 m. At a depth of 1000 m, the vertical stress is ~25 MPa with an average density of the overburden at 2500 kg m^{-3}. Under
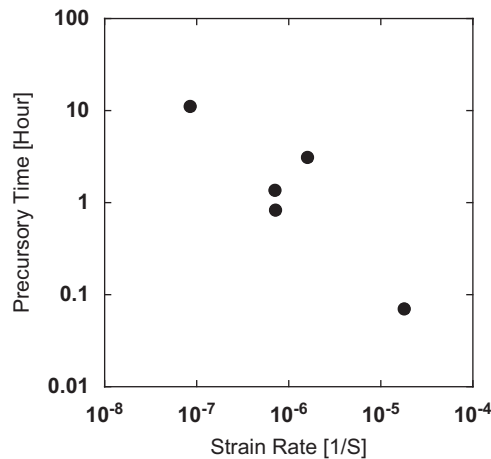
Fig. 12. Precursory time versus strain rate.

close, and then recovers as new vertical dilatant microcracks are generated. This occurs until the point of failure where permeability suddenly increases by 3–4 orders of magnitude. During loading, the point where permeability begins to increase occurs earlier than the switch in the volumetric strain from compaction to dilation. This phenomenon can be explained by the competing processes of axial crack opening and oblique and transverse crack closure.

The coal specimens tested in this study exhibit strain and permeability hysteresis when subjected to cyclic loading. Because new microcracks are generated, at the same deviatoric stress, a slight increase in permeability is observed during unloading. This is perhaps due to the temporary dominance of permeability response due to the nonaxial cracks. After each load-cycle, permeability does not change significantly suggesting that permeability is mainly controlled by the magnitude of the applied deviatoric stress rather than the numbers of load-cycles. With increasing stress, permeability during loading or after unloading is augmented once new cracks are created. This observation is analogous to the "Kaiser effect" where the development of failure is conditioned to a prior stress–memory in the sample.

Based on these laboratory observations, we propose a process-based model to describe the instability of underground coal seams. Horizontal stress, vertical stress, pore pressure, permeability, and desorption rate all redistribute around the mining-face as excavation progresses. Due to this redistribution, the closest zone near the mining-face may experience tensile failure if the permeability of the coal is low. Moving ahead of the face, there may exist a zone that can undergo overpressure and desorption-induced energetic failure. Further away from the face a shear failure zone may develop due to the large mining-induced stress that can also result in rapid failure if the desorption rate outstrips the rate of drainage. Then we scale our data to the field in space and time, providing useful reference for prediction.

Finally, we discuss how CO_2 injection reduces the effective stress, degrades coal strength, and thus may lead to instability of coal seams, and fault slip if faults are present. These instabilities may be accompanied gas outbursts. Seismic events or tectonic faulting may also trigger gas outbursts during long-term storage of CO_2 in underground coal seams.

this stress, the reduction in effective stress due to CO_2 injection increases the possibility of coal seam failure if the injection pressure is sufficiently high. Our results in this study show that at an effective stress of 1.5 MPa, coal fails at approximately 21 MPa. Although coal seam properties vary from site to site, CO_2 injection pressures should be chosen with caution at this depth. Previous studies have identified geological structures such as faults that exist in underground coal mines [1,3,4,10,32] and at some ongoing or planned CO_2 sequestration sites [68,69,70]. For CO_2 sequestration in underground coal seams with the presence of faults, the injection can reduce the effective stress, alter the permeability and state of sorption and swelling, degrade the mechanical properties of coal [26,43], and thus destabilize the formation, and eventually may reactivate fault slip or earthquakes. Different from other rock types, fault slips or earthquakes in coal seams have the potential to cause gas outbursts due to the large sorption capacity of CO_2 in coal [67]. In terms of long term storage of CO_2 in coal seams, even although the faults may not be reactivated during the injection period, tectonic faulting or earthquakes can still trigger rapid gas desorption from coal and possible dynamic and energetic rupture. Therefore, attention should be paid to the fault distribution when selecting carbon geological sequestration cites.

6. Conclusions

This study presents experimental data on the continuous evolution of permeability to water and gas of coal samples under prescribed confining stress and driven to failure (increasing deviatoric stress). Use of the constant pore pressure differential technique allows the continuous measurement of permeability evolution during progressive deformation through failure.

These experiments show that the coal is an elastic, brittle-plastic material with strain-weakening behavior. The stress–strain curves show typical behavior of coal with increasing strength with increasing effective confining stress. An initial non-linear portion of the curve is caused by the closing of the preexisting cleats in the coal and followed by a linear elastic response at intermediate stresses. A final non-linear portion develops due to pre-rupture cracking. The Young's modulus increases with increasing confining pressure, probably due to compaction of the coal, the increasing stiffness and the difference in sorption capacities.

For coal samples examined here, as differential stress and strain increase, permeability first decreases as pre-existing cleats

References

[1] Beamish BB, Crosdale PJ. Instantaneous outbursts in underground coal mines: an overview and association with coal type. Int J Coal Geol 1998;35:27–55.
[2] Cappa F, Rutqvist J. Impact of CO_2 geological sequestration on the nucleation of earthquakes. Geophys Res Lett 2011;38:L17313.
[3] Lama RD, Bodziony J. Management of outburst in underground coal mines. Int J Coal Geol 1998;35:83–115.
[4] Wold MB, Connell LD, Choi SK. The role of spatial variability in coal seam parameters on gas outburst behaviour during coal mining. Int J Coal Geol 2008;75:1–14.
[5] Xu T, Tang CA, Yang TH, Zhu WC, Liu J. Numerical investigation of coal and gas outbursts in underground collieries. Int J Rock Mech Min Sci 2006;43:905–19.
[6] Karacan CO, Ruiz FA, Cote M, Phipps S. Coal mine methane: a review of capture and utilization practices with benefits to mining safety and to greenhouse gas reduction. Int J Coal Geol 2011;86:121–56.
[7] Huang B, Liu C, Fu J, Guan H. Hydraulic fracturing after water pressure control blasting for increased fracturing. Int J Rock Mech Min Sci 2011;48:976–83.

[8] Diaz Aguado MB, Gonzalez Nicieza C. Control and prevention of gas outbursts in coal mines, Riosa-Olloniego coalfield Spain. Int J Coal Geol 2007;69:253–66.

[9] Lu T, Zhao Z, Hu H. Improving the gate road development rate and reducing outburst occurrences using the waterjet technique in high gas content outburst-prone soft coal seam. Int J Rock Mech Min Sci 2011;48:1271–82.

[10] Shepherd J, Rixon LK, Griffiths L. Outbursts and geological structures in coal mines: a review. Int J Rock Mech Min Sci 1981;18:267–83.

[11] Harpalani S. Gas Flow through Stressed Coal, PhD thesis, University of California, Berkeley, 1985, 158 pages.

[12] Gentzis T, Deisman N, Chalaturnyk RJ. Geomechanical properties and permeability of coals from the Foothills and Mountain regions of western Canada. Int J Coal Geol 2007;69:153–64.

[13] Hobbs DW. The strength and the stress–strain characteristics of coal in triaxial compression. J Geol 1964;72:214–31.

[14] Medhurst TP, Brown ET. A study of the mechanical behaviour of coal for pillar design. Int J Rock Mech Min Sci 1998;35:1087–105.

[15] Bieniawski ZT. The effect of specimen size on compressive strength of coal. Int J Rock Mech Min Sci 1968;5:325–35.

[16] Scholtes L, Donz F-V, Khanal M. Scale effects on strength of geomaterials, case study: coal. J Mech Phys Solids 2009;59:1131–46.

[17] Kaiser PK, Maloney SM. Deformation properties of a sub-bituminous coal mass. Int J Rock Mech Min Sci 1982;19:247–52.

[18] Das MN. Influence of width/height ratio on post-failure behaviour of coal. Geotech Geol Eng 1986;4:79–87.

[19] Okubo S, Fukui K, Qingxin Q. Uniaxial compression and tension tests of anthracite and loading rate dependence of peak strength. Int J Coal Geol 2006;68:196–204.

[20] Durucan S, Edwards JS. The effects of stress and fracturing on permeability of coal. Min. Sci. Tech 1986;3:205–16.

[21] Liu J, Chen Z, Elsworth D, Qu H, Chen D. Interactions of multiple processes during CBM extraction: a critical review. Int J Coal Geol 2011;87:175–89.

[22] Liu J, Wang J, Chen Z, Wang S, Elsworth D, Jiang Y. Impact of transition from local swelling to macro swelling on the evolution of coal permeability. Int J Coal Geol 2011;88:31–40.

[23] Pini R, Ottiger S, Burlini L, Storti G, Mazzotti M. Role of adsorption and swelling on the dynamics of gas injection in coal. J Geophys Res 2009;114:B04203.

[24] Siriwardane H, Haljasmaa I, McLendon R, Irdi G, Soong Y, Bromhal G. Influence of carbon dioxide on coal permeability determined by pressure transient methods. Int J Coal Geol 2009;77:109–18.

[25] Somerton WH, Soylemezoglu IM, Dudley RC. Effect of stress on permeability of coal. Int J Rock Mech Min Sci 1975;12:129–45.

[26] Wang S, Elsworth D, Liu J. Permeability evolution in fractured coal: the roles of fracture geometry and water-content. Int J Coal Geol 2011;87:13–25.

[27] Harpalani S, Chen G. Influence of gas production induced volumetric strain on permeability of coal. Geotech Geol Eng 1997;15:303–25.

[28] Harpalani S, Schraufnagel RA. Shrinkage of coal matrix with release of gas and its impact on permeability of coal. Fuel 1990;69:551–6.

[29] Hol S, Spiers CJ. Competition between adsorption-induced swelling and elastic compression of coal at CO_2 pressures up to 100 MPa. J Mech Phys Solids 2012;60:1862–82.

[30] Wang S, Elsworth D, Liu J. A mechanistic model for permeability evolution in fractured sorbing media. J Geophys Res 2012;117:B06205.

[31] Cao Y, He D, Glick DC. Coal and gas outbursts in footwalls of reverse faults. Int. J. Coal Geol 2001;48:47–63.

[32] Li H. Major and minor structural features of a bedding shear zone along a coal seam and related gas outburst, Pingdingshan coalfield, northern China. Int J Coal Geol 2001;47:101–13.

[33] Peng LS. Introduction to gas–geology. Beijing: China: Coal Industry Publishing House; 1990 [in Chinese].

[34] Klinkenberg LJ. The permeability of porous media to liquids and gases. In: Drilling and production practice. American Petroleum Institute, 1941. p. 200–213.

[35] Zhu WC, Liu J, Sheng JC, Elsworth D. Analysis of coupled gas flow and deformation process with desorption and Klinkenberg effects in coal seams. Int J Rock Mech Min Sci 2007;44:971.

[36] Jaeger JC, Cook NGW, Zimmerman RW. Fundamentals of rock mechanics. 4th ed. Oxford: Wiley-Blackwell; 2007.

[37] Cox SJD, Meredith PG. Microcrack formation and material softening in rock measured by monitoring acoustic emissions. Int J Rock Mech Min Sci 1993;30:11–24.

[38] He MC, Miao JL, Feng JL. Rock burst process of limestone and its acoustic emission characteristics under true-triaxial unloading conditions. Int J Rock Mech Min Sci 2010;47:286–98.

[39] Zhao Y, Jiang Y. Acoustic emission and thermal infrared precursors associated with bump-prone coal failureInt J Coal Geol 83:11-20.

[40] Bai M, Elsworth D. Coupled processes in subsurface deformation, flow, and transport. Reston, Virginia: ASCE Press; 2000.

[41] Elsworth D, Bai M. Flow-deformation response of dual-porosity media. J Geotech Eng 1992;118:107–24.

[42] Izadi G, Wang S, Elsworth D, Liu J, Wu Y, Pone D. Permeability evolution of fluid-infiltrated coal containing discrete fractures. Int J Coal Geol 2011;85:202–11.

[43] Wang S, Elsworth D, Liu J. Failure behavior of methane infiltrated coal: the role of gas desorption, confining stress and loading rate. Rock Mech Rock Eng in press.

[44] Konecny P, Kozusnikova A. Influence of stress on the permeability of coal and sedimentary rocks of the Upper Silesian basin. Int J Rock Mech Min Sci 2011;48:347–52.

[45] Mitchell TM, Faulkner DR. Experimental measurements of permeability evolution during triaxial compression of initially intact crystalline rocks and implications for fluid flow in fault zones. J Geophys Res 2008;113:B11412.

[46] Elsworth D, Goodman RE. Characterization of rock fissure hydraulic conductivity using idealized wall roughness profiles. Int J Rock Mech Min Sci 1986;23:233–43.

[47] Yeo IW, de Freitas MH, Zimmerman RW. Effect of shear displacement on the aperture and permeability of a rock fracture. Int J Rock Mech Min Sci 1998;35:1051–70.

[48] Shkuratnik V, Filimonov Y, Kuchurin S. Acoustic emission memory effect in coal samples under uniaxial cyclic loading. J Appl Mech Tech Phys 2006;47:236–40.

[49] Zoback MD, Byerlee JD. The effect of cyclic differential stress on dilatancy in Westerly granite under uniaxial and triaxial conditions. J Geophys Res 1975;80:1526–30.

[50] White CM, Smith DH, Jones KL, Goodman AL, Jikich SA, LaCount RB, et al. Sequestration of carbon dioxide in coal with enhanced coalbed methane recovery-a review. Energy Fuels 2005;19:659–724.

[51] Goodman AL, Campus LM, Schroeder KT. Direct evidence of carbon dioxide sorption on argonne premium coals using attenuated total reflectance-Fourier transform infrared spectroscopy. Energy Fuels 2004;19:471–6.

[52] Melnichenko YB, Radlinski AP, Mastalerz M, Cheng G, Rupp J. Characterization of the CO_2 fluid adsorption in coal as a function of pressure using neutron scattering techniques (SANS and USANS). Int J Coal Geol 2009;77:69–79.

[53] Hol S, Peach CJ, Spiers CJ. Applied stress reduces the CO_2 sorption capacity of coal. Int J Coal Geol 2011;85:128–42.

[54] Larsen JW. The effects of dissolved CO_2 on coal structure and properties. Int J Coal Geol 2004;57:63–70.

[55] Pan Z, Connell LD. A theoretical model for gas adsorption-induced coal swelling. Int J Coal Geol 2007;69:243–52.

[56] Hol S, Spiers CJ, Peach CJ. Microfracturing of coal due to interaction with CO_2 under unconfined conditions. Fuel 2012;97:569–84.

[57] Ouyang ZH, Li CH, Xu WC, Li HJ. Measurements of in situ stress and mining-induced stress in Beiminghe Iron Mine of China. J Centr S Univ Tech 2009;16:85–90.

[58] Singh AK, Singh R, Maiti J, Kumar R, Mandal PK. Assessment of mining induced stress development over coal pillars during depillaring. Int J Rock Mech Min Sci 2011;48:805–18.

[59] Yang W, Lin BQ, Qu YA, Li ZW, Zhai C, Jia LL, Zhao WQ. Stress evolution with time and space during mining of a coal seam. Int J Rock Mech Min Sci 2011;48:1145–52.

[60] Singh R, Singh TN, Dhar BB. Coal pillar loading in shallow mining conditions. Int J Rock Mech Min Sci 1996;33:757–68.

[61] Ates Y, Barron K. The effect of gas sorption on the strength of coal. Min Sci Tech 1988;6:291–300.

[62] Li X-Z, Hua A-Z. Prediction and prevention of sandstone-gas outbursts in coal mines. Int J Rock Mech Min Sci 2006;43:2–18.

[63] Sang S, Xu H, Fang L, Li G, Huang H. Stress relief coalbed methane drainage by surface vertical wells in China. Int J Coal Geol 2010;82:196–203.

[64] Brady BT. Anomalous seismicity prior to rock bursts: implications for earthquake prediction. Pure Appl Geophys 1977;115:357–74.

[65] Iannacchione A, Bajpayee TS, Edwards J. Forecasting roof falls with monitoring technologies—a look at the Moonee Colliery experience. In: Proceedings of the 24th international conference ground control in mining, Morgantown, WV, 2005. p. 44–60.

[66] Lama RD, Saghafi A. Overview of gas outburst and unusual emissions. In: Proceedings of the coal operators' conference; 2002. p. 74–88.

[67] Li T, Cai MF, Cai M. Earthquake-induced unusual gas emission in coalmines—A km-scale in-situ experimental investigation at Laohutai mine. Int J Coal Geol 2007;71:209–24.

[68] van Bergen F, Krzystolik P, van Wageningen N, Pagnier H, Jura B, Skiba J, et al. Production of gas from coal seams in the Upper Silesian Coal Basin in Poland in the post-injection period of an ECBM pilot site. Int J Coal Geol 2009;77:175–87.

[69] Pashin JC, McIntyre MR. Temperature-pressure conditions in coalbed methane reservoirs of the Black Warrior basin: implications for carbon sequestration and enhanced coalbed methane recovery. Int J Coal Geol 2003;54:167–83.

[70] Rutqvist J, Birkholzer J, Cappa F, Tsang CF. Estimating maximum sustainable injection pressure during geological sequestration of CO_2 using coupled fluid flow and geomechanical fault-slip analysis. Energy Convers Manage 2007;48:1798–807.